

01

Blazed silicon gratings for soft X-ray and extreme ultraviolet radiation: the effect of groove profile shape and random roughness on the diffraction efficiency

© L.I. Goray,^{1,2,3,4} V.A. Sharov,⁵ D.V. Mokhov,² T.N. Berezovskaya,² K.Yu. Shubina,² E.V. Pirogov,²
A.S. Dashkov,^{1,2} A.D. Bouravleuv^{1,3,4,5}

¹ Saint Petersburg Electrotechnical University „LETI“,
197022 St. Petersburg, Russia

² Alferov University,
194021 St. Petersburg, Russia

³ Institute for Analytical Instrumentation,
198095 St. Petersburg, Russia

⁴ University under the Inter-Parliamentary Assembly of EurAsEC,
194044 St. Petersburg, Russia

⁵ Ioffe Institute,
194021 St. Petersburg, Russia

e-mail: lig@pcgrate.com

Received March 31, 2023

Revised March 31, 2023

Accepted March 31, 2023

The effect of the groove profile shape and random roughness of the reflecting facet of five silicon diffraction gratings (1–4° blaze angle, period 0.4, 1.4, 2, and 4 μm, various coatings) operating in the soft X-ray and extreme ultraviolet radiation ranges on the outflow of the diffraction efficiency from working orders is studied. Diffraction gratings were fabricated by wet etching of Si(111) vicinal wafers and characterized by atomic force microscopy to determine the shape of the groove profile and roughness. The diffraction efficiency of gratings operating in classical and conical diffraction mounts was calculated based on realistic groove profiles by computer simulation using the PCGrate™ code and taking into account the scattering intensity using Nevot-Croce or Debye-Waller corrections or using the Monte Carlo method (rigorously). The effect of the groove profile shape and roughness on the diffraction efficiency of the fabricated Si gratings is shown.

Keywords: diffraction grating, triangular groove profile, reflective facet roughness, AFM, diffraction efficiency modelling.

DOI: 10.61011/TP.2023.07.56619.66-23

Introduction

The aim of the present study is to estimate the spread of the groove profile shape over the grating aperture and the permissible roughness of the reflecting facet that do not exert a significant influence on the maximum attainable diffraction efficiency of gratings operating in the soft X-ray (SXR) and extreme ultraviolet (EUV) ranges in classical and conical diffraction mounts. The values of efficiency determined using a computer code (PCGrate™ and Monte Carlo modeling of the scattering intensity) with the inclusion of random roughness relief and without it are compared for this purpose [1,2]. The correctness of model efficiency values is normally verified by comparing them to reflectometry data. It has been demonstrated in our study [3] that the results of modeling relying on the method of boundary integral equations and the results of reflectometric determination of the grating efficiency agree well (specifically, in the case when the influence of random roughness on the outflow of

diffraction efficiency from working orders is taken into account).

No studies of this type have been performed earlier; the allowed root-mean-square (RMS) roughness σ of the reflecting facet was typically estimated as $\sigma \ll \lambda/6 \cos \theta$ [4], where λ is the incident radiation wavelength and θ is the incidence angle measured from the normal. The following values of σ of the grating surface are considered acceptable: ~ 0.5 – 1 nm [5] for applications in EUV and ~ 0.3 – 0.4 nm [6] for the SXR range. The influence of the groove profile shape and random surface roughness of the reflecting facet on the outflow of diffraction efficiency from the working order was examined for SXR and EUV radiation and Si gratings with a blaze angle of 1–4°, periods of 0.4, 1.4, 2, and 4 μm, and various coatings. Gratings were designed to be operated within the SXR wavelength range of 0.6–1.4 nm and at EUV wavelengths of 11.3, 13.6, 17.1, and 30.4 nm. The studied diffraction gratings were fabricated by wet etching of vicinal (111) silicon wafers following an improved procedure that was detailed in [7,8].

1. Theory of scattering off random roughness

The development of a rigorous electromagnetic (EM) theory of (elastic) scattering of light by particles and irregularities (roughness) was initiated in the middle of the 20th century when computers and the corresponding mathematical theories and numerical techniques became available. Only a handful of exact solutions of diffraction problems for individual elements (circular cylinder (Rayleigh, 1882), perfect half-plane (Sommerfeld, 1896), and sphere (Mie, 1908)) were known at the time. At present, if wave number k and characteristic size a of a scatterer are related as $ka \ll 1$ (Rayleigh approximation) or $ka \gg 1$ (geometric optics, scalar Kirchhoff integral), one may find a great number of elegant and efficient analytical, semi-analytical, and rapidly converging numerical solutions of diffraction problems for various obstacles in different fields of study. The Born approximation (BA), the distorted-wave Born approximation (DWBA), and the Beckman–Spizzichino theory may serve as examples in the short-wave range.

In what follows, the X-ray range is understood as radiation with wavelength λ ranging from ~ 0.04 to ~ 60 nm (i.e., hard X-ray (HXR), SXR, and EUV combined). The exploration of the X-ray range began at HXR wavelengths: the theory of X-ray diffraction in crystals has been developed already in the early 20th century by Ewald, Bragg, Darwin, and Prince. About 20 Nobel Prizes have been awarded in the last century to researchers who made discoveries in this range. Following the advent of thin-film coatings in the middle of the 20th century, the simplest optical theories characterizing similar phenomena from a different standpoint (that of Maxwell equations) have been outlined for the first time in the works of Abeles, Vlasov, Rouard, Heavens, Parratt, and Brekhovskikh. The dynamic theory of X-ray scattering in its complete and precise formulation yields the same results as the corresponding optical theory (i.e., these theories are equivalent). However, since the EM theory is more versatile in nature and numerical methods and computers have enjoyed an enormous progress, studies relying on EM methods become more and more important in the X-ray range.

Multiple diffraction, refraction, absorption, waveguide effects, and deformation of fronts largely govern the scattering of SXR and EUV radiation and cold neutrons by nanoirregularities of continuous media and layers. The inclusion of these purely dynamic effects, which requires the application of the EM theory, provides an opportunity to calculate the absolute intensity of mirror and diffuse components, which may have resonance peaks. However, if the sizes of irregularities differ by 3–5 orders of magnitude (e.g., in the case of a diffraction grating with period $d \sim 1\text{--}10\ \mu\text{m}$ and RMS roughness $\sigma \sim 1\text{--}0.1$ nm), accurate characterization of diffraction turns into a serious computational challenge even for modern workstations.

The Debye–Waller (DW) amplitude correction,

$$r_{\text{DW}}(k) = \exp\{-2(2\pi\sigma(k) \cos \theta_k/\lambda)^2\},$$

characterizing the outflow of power from the mirror component at roughness (diffuseness) of the interface with number k is known from BA. It is used more often in the region when incidence angle θ_k measured from the normal to the surface is smaller than the critical angle. Another model with the Nevot–Croce (NC) coefficient,

$$r_{\text{NC}}(k) = \exp[-2(2\pi\sigma(k)/\lambda)^2 n_{k+1} \cos \theta_{k+1} n_k \cos \theta_k],$$

which is derived from DWBA, is commonly used at grazing incidence beyond the critical angle from a medium with real part n_k of the refraction index. Both factors of attenuation of mirror reflection are valid in the case of a Gaussian roughness and a Gaussian autocorrelation function at, strictly speaking, a low boundary roughness height h and a very large (DW) or very small (NC) correlation length ξ [4,9,10]. All approximations feature severe restrictions, especially on the maximum values of h [11–14]. DWBA is commonly applied to arbitrary h values; by definition, however, this approximation is valid only at $h \cos \theta/\lambda \ll 1$ and $\xi k \cos^2 \theta \ll 1$, where λ is the wavelength in vacuum. It is known that second-order DWBA and roughness-height perturbation theory may be used in the context of an arbitrary correlation length and more general roughness statistics. However, parameters σ and ξ become insufficient for characterization of the intensity distribution of the diffuse component when $\sigma \cos \theta > \lambda/10$ [15].

A new approach in short-wave reflectometry relying on the rigorous theory of diffraction of EM radiation and utilizing the method of boundary integral equations and the Monte Carlo method [1,16] has been proposed relatively recently, when convergence of the corresponding equations for $\lambda/\xi \sim 10^{-6}$ was achieved [17,18]. Such rigorous calculations of the intensity of scattering by random roughness with accurate characterization of absorption are referred to as deep X-ray reflectometry (DXRR) in literature [19,20]. The DXRR method may provide an accurate description of all phenomena ranging from total internal reflection to complete absorption of short-way radiation. In addition to mirror reflection coefficients, it allows one to determine accurately the intensity of scattered radiation and absorption [21]. This method and the PCGrate™ code [22] were used to calculate the coefficients of mirror and diffuse (diffraction) reflection off single-layer Ge/Si [23] and multilayer (multiplied) In(Ga)As/GaAs quantum dots (islands) [24]; gold rough mirrors [4,21]; rough GaAs substrates [19,20] and multilayer Al(Ga)As/GaAs heterostructures [25]; multilayer X-ray Mo/Si and Al/Zr mirrors [9,10]; WB₄/C and Cr/C diffraction gratings (based on the data from a model of growth of realistic boundaries at arbitrary roughness statistics) [26]; the surface of a hydrosol with 10 nm SiO₂ particles enriched with CsOH [27]; and bulk and multilayer gratings with a measured roughness of boundaries [1,21,28].

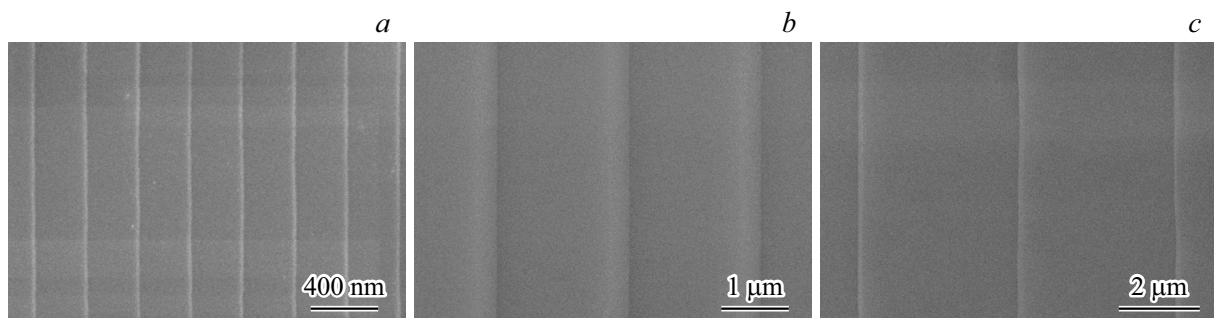


Figure 1. SEM images of the grating surface: *a* — Sv-1, 100 K; *b* — Si-p-6, 50 K; *c* — Si-13-2, 30 K.

Significant differences (including those in the magnitude of reconstructed roughness parameters) between the rigorous approach and the application of corrections were revealed in the case of mirror (Bragg) reflection coefficients of Au and multilayer mirrors with various roughness statistics within a wide range of wavelengths and incidence angles [4,10].

2. Parameters of grating grooves and methods for characterization and simulation of efficiency

In order to determine the parameters of a grating, its profile is recorded over a length of 10 periods in several regions (depending on the grating size). The efficiency is then calculated using specialized software tools and averaged parameters of the grating and reflective coating layers. The parameters of studied gratings (all fabricated on wafers with a thickness of 1.5 mm, except for grating Si-13-2 with a thickness of ~ 0.4 mm) are listed in Table 1. The type of reflective coating and the blazed wavelength are indicated in the last column. Gratings with a gold or platinum coating may operate both in classical and conical diffraction mounts in EUV and SXR ranges, while gratings with multilayer coatings are designed to be used in the classical setup at EUV wavelengths. A proper multilayer coating (period Λ and layer thicknesses) was selected with account for the chosen wavelength (range) and parameters of fabricated gratings, with the most important of them being the groove period and the blaze angle (i.e., groove depth). The potential for operation in high spectrum orders, which is governed by planarity and the working facet length, was also taken into account [29].

Figure 1 presents the images of surfaces of several fabricated gratings obtained under different magnifications using a Supra25 scanning electron microscope (SEM).

Figure 2 shows the photographic image of grating Si-p-3 fabricated on a silicon wafer 76.2 mm in diameter.

Roughness. High-frequency and medium-frequency (waviness) roughness components, which scatter incident radiation, are found on the surface of a reflecting facet of a Si grating. High-frequency (σ) roughness was measured with an atomic force microscope in a $1 \times 1 \mu\text{m}^2$ field, while

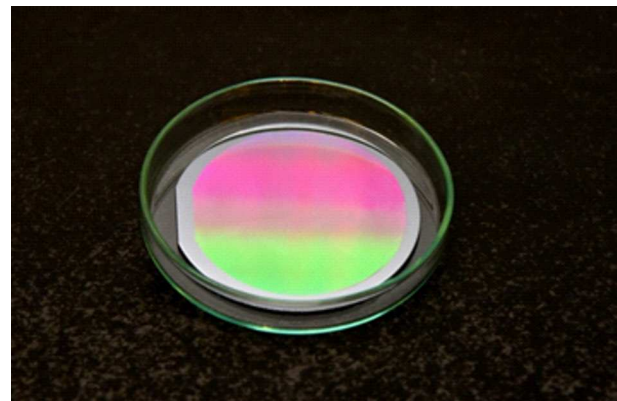


Figure 2. Structure photo of the Si-p-3 grating.

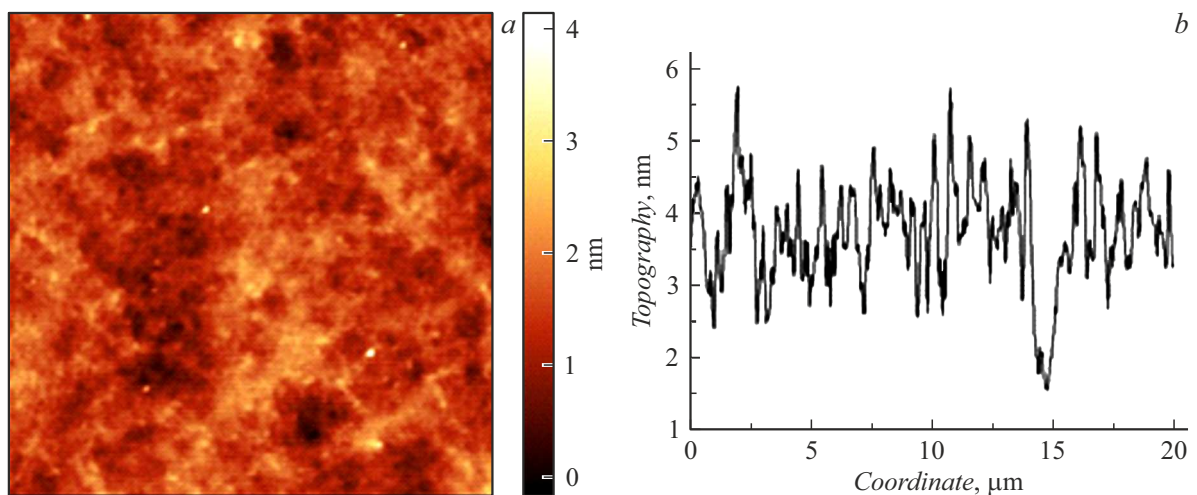
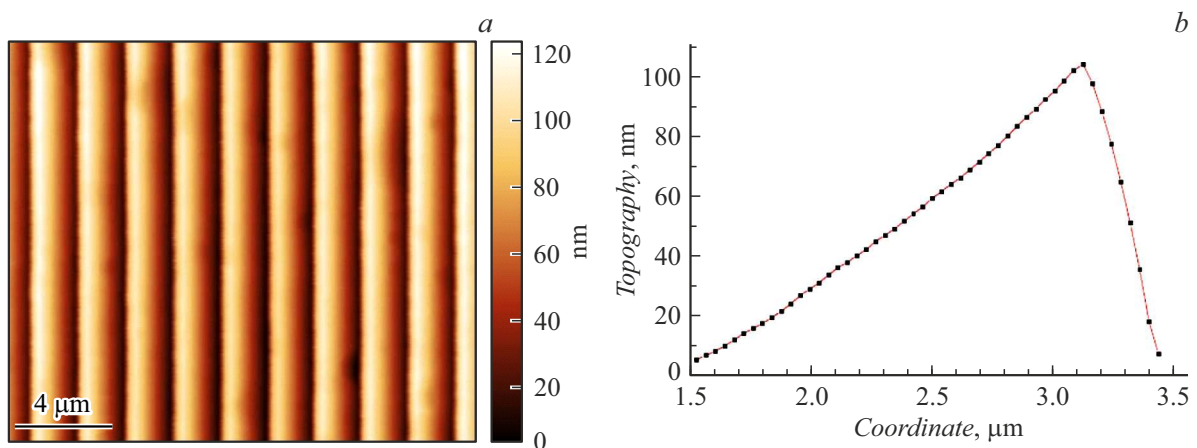
medium-frequency roughness (R_q) was determined within a length of $20 \mu\text{m}$ along a groove on the surface of a reflecting facet (Fig. 3). Roughness calculations were performed using the Gwyddion code [30].

Averaged profile. A field containing ten periods of a grating was scanned to determine the grating parameters listed in Table 1. An example AFM topography of a $20 \times 20 \mu\text{m}^2$ field for a grating with a period of $2 \mu\text{m}$ is shown in Fig. 4, *a*. Scanning was performed in the transverse (i.e., perpendicular to the grooves) direction in order to suppress artifacts. A profile averaged over 128 scan lines, which is representative of certain averaged parameters of a grating, may be derived from these scans [31]. In order to obtain a realistic averaged profile of a single groove for efficiency modeling, a similar procedure was performed in a field with a length of 1.5 grating periods, and points definitely corresponding to a single period were selected from this field. A scan size reduction is needed to raise the number of groove profile sampling points and characterize random roughness. An example averaged profile of a single groove of a grating with a period of $2 \mu\text{m}$ is shown in Fig. 4, *b*. A similar profile was used in PCGrate™ to calculate the diffraction efficiency.

Random profile. Several non-averaged AFM scans of grating groove profiles containing a few periods are used to characterize random roughness accurately. In the present

Table 1. Parameters of gratings

Sample No.	Period, μm	Working facet length, nm	Working facet tilt, deg	Working facet curvature, deg	Nonworking facet tilt, deg	RMS roughness, nm		Reflective coating type/blazed wavelength, nm
						σ $1 \times 1 \mu\text{m}^2$	R_q $20 \mu\text{m}$	
Sv-1	0.4	339	3.9	—	28	0.34	2.20	Mo–Be/11.3
Si-p-8-2	1.4	1085	3.9	0.74	15	0.58	4.38	Au/11.3, 0.8
Si-p-6	2.0	1600	3.5	0.80	19	0.42	2.72	Au/17.1
Si-p-3	4.0	3677	3.4	0.57	28	0.49	1.19	Be–Mg/30.4
Si-13-2	4.0	3191	1.2	0.81	10	0.55	2.40	Pt/13.6

**Figure 3.** Roughness of the reflecting facet of a grating: *a* — AFM topography, $\sigma = 0.35$ nm; *b* — surface scan, $R_q = 0.77$ nm.**Figure 4.** Modeled grating with a period of $2 \mu\text{m}$: *a* — AFM topography of a region $20 \times 20 \mu\text{m}^2$ in size; *b* — profile of an averaged grating groove.

study, random groove profiles were measured over a length of three periods in different grating regions with a large number of sampling points (at a minimum scan rate). All heights and spatial frequencies of a statistically rough surface (commonly defined by σ , R_q , and ξ), which affect

the scattering of incident radiation if its wavelength is comparable to the roughness amplitude (with an allowance made for the incidence angle), are taken into account in the mode of scanning with a large number of profile sampling points. This approach provides an opportunity to use the

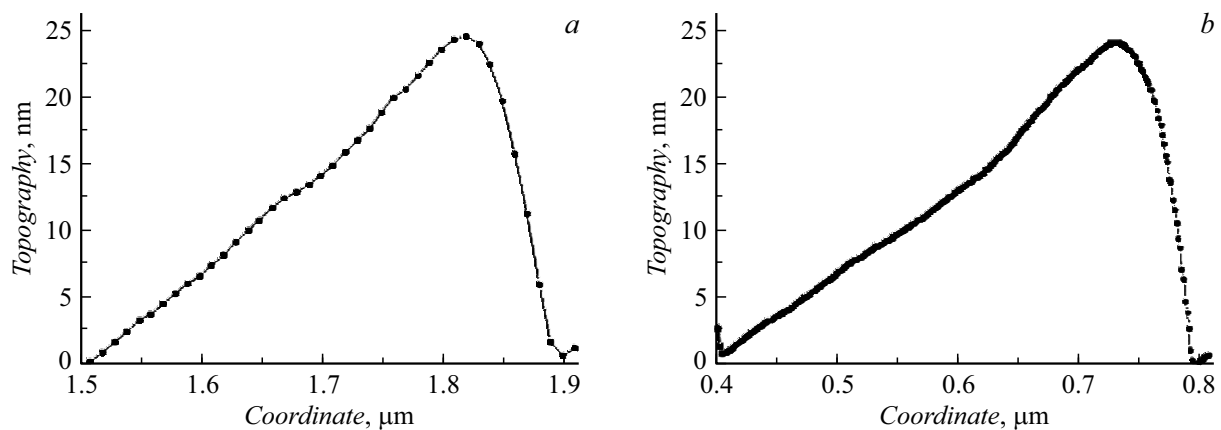


Figure 5. Profiles of one groove of grating Sv-1 measured: *a* — with an average number of sampling points; *b* — with a large number of sampling points.

obtained statistical groove profiles in rigorous Monte Carlo calculations of the efficiency and the intensity of scattered radiation.

Figure 5 shows the random profiles of a single period for high-frequency grating Sv-1 measured with average and large numbers of sampling points (i.e., with average and low profile measurement rates). An NTegra Aura (Russia) atomic force microscope was used to scan profiles and measure the grating surface roughness.

Efficiency modeling. The absolute diffraction efficiency of the studied gratings was modeled using the obtained realistic (averaged and sets of random) groove profiles and radiation with the following wavelengths: 0.6–1.4, 11.3, 13.6, 17.1, 30.4 nm. The efficiency was determined in PCGrateTM v.6.7.1 [22].

An averaged grating groove profile (Fig. 4, *b*) was used to model the efficiency without regard to roughness. An averaged groove profile and NC or DW corrections for the obtained σ roughness values [16,31] were applied in efficiency modeling with approximate characterization of interface roughness. Monte Carlo modeling of the efficiency with rigorous characterization of high-frequency (σ) and medium-frequency (R_q) roughness and arbitrary roughness statistics was performed with the use of several sets of measured (non-averaged) groove profiles with a few periods taken from different grating regions.

3. Numerical modelling results and discussion

Table 2 lists the maximum absolute efficiency values of the studied gratings in unpolarized radiation both in classical (radiation is incident on a grating and reflected into orders within the dispersion plane (perpendicular to grooves)) and conical (radiation is incident on a grating along its grooves at a polar angle equal to the blaze angle and is reflected into orders arranged in a cone) diffraction mounts [1,32]. The efficiencies at maxima of orders of

grating Si-p-6 at a wavelength of 17.1 nm and grating Si-p-3 at a wavelength of 30.4 nm calculated for the classical mount without regard to roughness and with approximate characterization of it are almost equal (the difference is $\leq 1\%$). The applicability criteria of roughness corrections are satisfied by a large margin for these EUV gratings with low σ . Thus, there is no need to perform rigorous Monte Carlo calculations, and such data are lacking in Table 2. Likewise, the maximum efficiencies for grating Si-p-8-2 with a gold coating at $\lambda = 11.3$ nm and grating Si-13-2 with a platinum coating at $\lambda = 13.6$ nm calculated for the classical mount without regard to roughness and with approximate characterization of it differ insignificantly (the difference does not exceed 1–2%). At $\lambda = 0.8$ nm, the difference between efficiencies calculated with and without regard to roughness for grating Si-p-8-2 operated in the conical mount is of the same order of magnitude: $\leq 1.8\%$, which is also insignificant. However, the results of Monte Carlo modeling with rigorous characterization of scattering off realistic groove profiles with random roughness reveal a much more considerable efficiency reduction for grating Si-p-8-2. Specifically, the diffraction efficiency at $\lambda = 11.3$ nm in the classical mount calculated with rigorous characterization of roughness is 4.1% lower in the -3 rd order and decreases by a factor of more than 2 in the -5 th order.

Such significant differences are attributable to a considerable medium-frequency roughness of the reflecting surface ($R_q = 4.38$ nm), which is neglected in the approximate approach (only the high-frequency roughness component is taken into account) and exerts a strong influence on the maximum diffraction efficiency and/or its redistribution among orders. Even at $\sigma = 2.32$ nm, which is four times higher than the AFM high-frequency roughness estimate, the results of approximate calculations for grating Si-p-8-2 reveal only a 2% reduction in efficiency of the -3 rd order. The differences between rigorous and approximate approaches observed for high-frequency multilayer grating Sv-1 under the assumption of vertical correlation of boundaries and roughness are even greater. Owing to significant

Table 2. Results of modeling of the absolute efficiency

Grating/coating/ Λ , nm	Parameters of efficiency modeling		Maximum absolute diffraction efficiency in unpolarized radiation, %		
	mount/wavelength, nm	diffraction order	without regard to σ and R_q	with regard to σ , approximate	with regard to σ and R_q , Monte Carlo
Sv-1/20xMo-Be/11.4	Classical/11.3	-1	1.7	2.6	18.0
		-2	6.4	3.1	28.2
		-3	42.3	29.5	37.0
		-4	18.5	24.5	6.1
Si-p-8-2/Au	Classical/11.3	-1	12.1	12.1	15.1
		-2	19.4	19.4	23.7
		-3	29.7	29.5	25.6
		-4	29.5	29.2	18.8
		-5	24.8	24.4	10.3
	Conical/0.8 nm	-1	61.7	61.6	–
		-2	57.6	57.3	–
		-3	51.5	50.9	–
		-4	45.7	44.7	–
		-5	39.4	38.8	–
		-6	33.7	32.6	–
		-7	28.2	26.4	–
		-8	22.4	20.6	–
Si-13-2/Pt	Classical/13.6 nm	-1	54.0	54.0	–
		-2	37.5	35.8	–
		-3	19.5	17.5	–
		-4	13.1	12.2	–
Si-p-3/10xBe-Mg/32.16	Classical/30.4 nm	-6	1.8	1.7	–
		-7	8.0	7.9	–
		-8	28.8	28.0	–
		-9	23.2	22.2	–
		-10	5.0	4.6	–
Si-p-6/Au	Classical/17.1 nm	-1	13.4	13.3	–
		-2	23.2	23.2	–
		-3	29.5	29.4	–
		-4	25.1	25.0	–
		-5	18.6	18.5	–
		-6	11.8	11.8	–

variations of the groove profile shape over the grating aperture and even the profile shape of individual grooves within the same AFM scan, the efficiency of orders and the intensity of scattered radiation vary greatly (by up to an order of magnitude) when one or the other realistic groove profile is taken into account. It follows from Table 2 that the approximate characterization of roughness is inadequate in the case of a high-frequency grating with a shallow depth and a wide spectrum of correlation lengths. Numerous statistical profile measurements and rigorous calculations are needed to process the results correctly in such cases.

Conclusion

The groove profile shape and random roughness of five diffraction gratings with different periods, blaze angles, and coatings were examined in detail. The studied gratings were fabricated by wet etching of vicinal Si(111) wafers and are designed for application in SXR and EUV radiation ranges. Statistically averaged and random groove profiles measured by AFM were used to model the absolute diffraction efficiency based on the rigorous method of boundary integral equations and the Monte Carlo method in PCGrateTM. The results obtained with accurate characterization of random roughness were compared to the approximate approach utilizing Nevot–Croce or Debye–Waller corrections. Although accurate calculations require considerable computer resources, modeling data are not only comparable to the results of synchrotron measurements, but also allow one to determine the magnitude of error corresponding to the use of any approximations. In addition, this approach is the only feasible one if the medium-frequency roughness component is to be taken into account. Our studies demonstrated that this is especially important in modeling of the efficiency of high-frequency gratings (with a period of several hundred nanometers) and gratings with a period on the order of one micrometer. Although the fabricated Si gratings had an almost perfect triangular profile and low RMS roughness values, parameter σ characterizes only the contribution of the high-frequency roughness component. Therefore, additional parameters (in the present case, R_q) and studies are needed to determine accurately the roughness statistics of an examined surface and utilize the data correctly in modeling of the diffraction efficiency of gratings with a realistic groove profile with random roughness taken into account.

Funding

The experimental work of L.I. Goray, A.S. Dashkov, D.V. Mokhov, E.V. Pirogov, and K.Yu. Shubina was supported by the Russian Science Foundation (19-12-00270-P). Numerical calculations were carried out with support from the Russian Foundation for Basic Research (19-29-12053-mk).

Conflict of interest

The authors declare that they have no conflict of interest.

References

- [1] L.I. Goray, G. Schmidt. In: *Gratings: Theory and Numerical Applications*, ed. by E. Popov (Institut Fresnel, AMU, 2014), p. 447.
- [2] L. Goray, M. Lubov. *J. Appl. Cryst.*, **46**, 926 (2013). DOI: 10.1107/S0021889813012387
- [3] L.I. Goray, T.N. Berezovskaya, D.V. Mokhov, V.A. Sharov, K.Yu. Shubina, E.V. Pirogov, A.S. Dashkov, A.V. Nashchekin, M.V. Zorina, M.M. Barysheva, S.A. Garakhin, S.Yu. Zuev, N.I. Chkhalo. *Bull. of the Lebedev Phys. Inst.* **50**(2) S250 (2023). <https://link.springer.com/article/10.3103/S1068335623140063>
- [4] L.I. Goray. *J. Appl. Phys.*, **108**, 033516 (2010). DOI: 10.1063/1.3467937
- [5] D.L. Voronov, E.H. Anderson, R. Cambie, F. Salmassi, E.M. Gullikson, V.V. Yashchuk, H.A. Padmore, M. Ahn, C.-H. Chang, R.K. Heilmann, M.L. Schattenburg. *Proc. SPIE*, **7448**, 74480J (2009). DOI: 10.1117/12.826921
- [6] L. Golub, P. Cheimets, E.E. DeLuca, C.A. Madsen, K.K. Reeves, J. Samra, S. Savage, A. Winebarger, A.R. Brucoleri. *J. Space Weather Space Clim.*, **10**, 37 (2020). DOI: 10.1051/swsc/2020040
- [7] L.I. Goray, T.N. Berezovskaya, D.V. Mokhov, V.A. Sharov, K.Yu. Shubina, E.V. Pirogov, A.S. Dashkov. *Tech. Phys.*, **92**(13), 2097 (2022). DOI: 10.21883/JTF.2021.10.51368.81-21
- [8] D.V. Mokhov, T.N. Berezovskaya, K.Yu. Shubina, E.V. Pirogov, A.V. Nashchekin, V.A. Sharov, L.I. Goray. *Tech. Phys.*, **92**(8), 1009 (2022). DOI: 10.21883/JTF.2022.08.52782.74-22
- [9] L. Goray, M. Lubov. *J. Surf. Invest. X-ray Synchrotron Neutron Tech.*, **8**(3), 444 (2014). DOI: 10.1134/S1027451014030057
- [10] L. Goray, M. Lubov. *Opt. Express*, **23**(8), 10703 (2015). DOI: 10.1364/OE.23.010703
- [11] J.A. Ogilvy. *Rep. Prog. Phys.*, **50**, 1553 (1987). DOI: 10.1088/0034-4885/50/12/001
- [12] D.K.G. de Boer. *Phys. Rev. B*, **51**, 5297 (1995). DOI: 10.1103/PhysRevB.51.5297
- [13] D.G. Stearns, D.P. Gaines, D.W. Sweeney, E.M. Gullikson. *J. Appl. Phys.*, **84**(2), 1003 (1998). DOI: 10.1063/1.368098
- [14] I.V. Kozhevnikov, M.V. Pyatakhin. *J. X-ray Sci. Tech.*, **8**(4), 253 (1998).
- [15] M. Saillard, D. Maystre, J.P. Rossi. *Opt. Acta*, **33**, 1193 (1986).
- [16] L.I. Goray. *Nucl. Instrum. Methods. Phys. Res. A*, **536**(1–2), 211 (2005). DOI: 10.1016/j.nima.2004.07.173
- [17] L. Goray. *Proc. SPIE*, **6617**, 661719 (2007). DOI: 10.1117/12.726038
- [18] L. Goray. *Proc. SPIE*, **7390**, 73900V (2009). DOI: 10.1117/12.827444
- [19] L.I. Goray, E.V. Pirogov, M.S. Sobolev, N.K. Polyakov, A.S. Dashkov, M.V. Svechnikov, A.D. Bouravlev. *Tech. Phys.*, **65**(11), 1822 (2020). DOI: 10.1134/S1063784220110134
- [20] L. Goray, E. Pirogov, M. Sobolev, I. Ilkiv, A. Dashkov, E. Nikitina, E. Ubyivovk, L. Gerchikov, A. Ipatov, Yu. Vainer, M. Svechnikov, P. Yunin, N. Chkhalo, A. Bouravlev. *J. Phys. D: Appl. Phys.*, **53**, 455103 (2020). DOI: 10.1088/1361-6463/aba4d6]

- [21] L. Goray. *J. Synchrotron Radiat.*, **28**, 196 (2021). DOI: 10.1107/S160057752001440X
- [22] I.I.G., Inc. [Electronic source]. Available at: URL: <http://pcgrate.com>, open access (date of access: 03.06.2023).
- [23] L.I. Goray, N.I. Chkhalo, Yu.A. Vainer, *Tech. Phys. Lett.*, **36**(2), 108 (2010). DOI: 10.1134/S1063785010020057
- [24] L.I. Goray, N.I. Chkhalo, G.E. Tsyrlin. *Tech. Phys.*, **54**, 561 (2009). DOI: 10.1134/S1063784209040185
- [25] L.I. Goray, E.V. Pirogov, M.V. Svechnikov, M.S. Sobolev, N.K. Polyakov, L.G. Gerchikov, E.V. Nikitina, A.S. Dashkov, M.M. Borisov, S.N. Yakunin, A.D. Bouravleuv. *Tech. Phys. Lett.*, **47**(10), 757 (2021). DOI: 10.1134/S1063785021080071
- [26] M. Lubov, L. Goray. *J. Synchrotron Rad.*, **26**, 1539 (2019). DOI: 10.1107/S1600577519006337
- [27] L.I. Goray, V.E. Asadchikov, B.S. Roshchin, Yu.O. Volkov, A.M. Tikhonov. *OSA Continuum*, **2**(2), 460 (2019). DOI: 10.1364/OSAC.2.000460
- [28] L.I. Goray, J.F. Seely. *Appl. Opt.*, **41**(7), 1434 (2002). DOI: 10.1364/AO.41.001434
- [29] L.I. Gorai, T.N. Berezovskaya, D.V. Mokhov, V.A. Sharov, K.Yu. Shubina, E.V. Pirogov, A.S. Dashkov. *Poverkhn.: Rentgenovskie, Sinkhrotronnye Neitr. Issled.*, **8**, 3 (2023) (in Russian).
- [30] Gwyddion download [Electronic source]. Available at: <http://gwyddion.net/download.php>, open access (date of access: 05.22.2023).
- [31] L.I. Goray, In: *Recent Developments in Atomic Force Microscopy and Raman Spectroscopy for Materials Characterization*, ed. by C.S. Pathak, S. Kumar (IntechOpen, 2022), 274 p. DOI: 10.5772/intechopen.94185
- [32] L. Goray, W. Jark, D. Eichert. *J. Synchrotron Radiat.*, **25**, 1683 (2018). DOI: 10.1107/S1600577518012419

Translated by D.Safin